ENGINEERING

Soft multifunctional bistable fabric mechanism for electronics-free autonomous robots

Dezhi Yang[1], Miao Feng[1], Jianing Sun[1], Yexun Wei[1], Jiang Zou[1,2], Xiangyang Zhu[1,2]*, Guoying Gu[1,2]*

Pneumatic soft robots are promising in diverse applications while they typically require additional electronics or components for pressure control. Fusing pneumatic actuation and control capabilities into a simple soft module remains challenging. Here, we present a class of bistable fabric mechanisms (BFMs) that merge soft bistable actuators and valves for electronics-free autonomous robots. The BFMs comprise two bonding fabric chambers with embedded tubes, where the straightening of one chamber compels the other to buckle for the bistability of the structure and the switching of the tube kinking. Our BFMs can facilitate fast bending actuation (more than 1166° s^{-1}), on/off and continuous pressure regulation, pneumatic logic computations, and autonomous oscillating actuation (up to 4.6 Hz). We further demonstrate the capabilities of BFMs for diverse robotic applications powered by one constant-pressure air supply: a soft gripper for dynamic grasping and a soft crawler for autonomous jumping. Our BFM development showcases unique features and huge potential in advancing entirely soft, electronics-free autonomous robots.

INTRODUCTION

Pneumatic soft robots have drawn extensive attention owing to their safety, adaptability, simplicity, practicability, and low cost (*1*). Benefiting from these advantages, they have shown tremendous promise and diverse applications, such as biomimetic robots (*2*–*6*), soft grippers (*7*–*10*), and wearable devices (*11*–*15*). However, pneumatic soft robots, especially those composed of multiple actuators, typically require several hard electronic valves and control modules for pressure control (*16*), which limits their integration of fully soft components. Moreover, their applications may be hindered in environments where electronics are prone to failure, such as underwater or high-radiation zones.

To achieve electronics-free autonomy in pneumatic soft robots, researchers have predominantly focused on assembling multiple classes of soft actuators and control modules. During the past decade, various soft actuators have been developed using elastomers, polymers, and fabrics, which enable a range of actuation motions including extension, contraction, bending, twisting, and hybrid movements (*17*–*23*). On the other hand, soft control modules have been reported through the development of pneumatic inverters (*24*–*26*), soft valves (*27*, *28*), membranes with slits (*29*, *30*), and narrow tubes with viscous flow (*31*, *32*). These soft control modules have been successfully used to design pneumatic logic gates, oscillators, nonvolatile memory storage, and pressure regulators (*28*, *33*–*40*), generating pressure signal sequences analogous to electronic circuit currents. In this sense, electronics-free soft robots can be conveniently realized through their combinations (*41*, *42*). However, these developments usually depend on different components for actuation and control, resulting in cumbersome fabrication and difficulties of integration.

In tackling these challenges, one promising strategy is to integrate actuation and control capabilities into a unified design (*28*, *38*, *43*, *44*). As a promising attempt, Lee *et al.* (*38*) used the inherent interactions between the buckling-sheet ring oscillator and the surroundings to achieve multimodal locomotion robots. Besides, Jiao *et al.* (*43*) presented soft origami LEGO with actuation, computation, and sensing capabilities to develop intelligent soft turtle robots. Recently, Decker *et al.* (*28*) introduced programmable soft valves with inner piston actuators for linear actuation of untethered robots. Despite the accumulative results, it remains challenging to fuse the actuation and control capabilities into a simple and efficient soft module.

Alternatively, snap-through bistability has been widely used to develop high-performance soft bistable actuators or valves, but not both simultaneously (*45*). They typically combine separate pneumatic actuators with bistable structures (*46*–*49*), or couple tube kinking with bistable membrane deformation (*27*, *50*). While directly combining existing bistable structures, pneumatic actuators, and tubes might offer a solution, it generally requires complicated configurations. Accordingly, the key challenge lies in the design of simple soft bistable structures and actuators, whose deformation can be inherently coupled with pneumatic components for control.

Here, we present a class of bistable fabric mechanisms (BFMs) that merge soft bistable actuators and valves by partially bonding two fabric chambers and embedding tubes. Controlling the pressures in the two chambers, the BFMs exhibit bistability with tunable energy barriers and can transition between stable states rapidly. In each stable state, one chamber straightens while the other buckles, causing the corresponding embedded tubes to be unkinked or kinked. We demonstrate that our BFMs can be configured as bistable actuators with fast bending actuation (more than 1166° s^{-1}), pneumatic circuit switches (PCSs) for interaction control, and pneumatic logic gates for autonomous control. Notably, a single BFM can multiplex the actuator and valve functions to achieve autonomous oscillating actuation (up to 4.6 Hz). Further, we develop a soft gripper capable of detecting objects and performing dynamic grasping and a soft crawler that jumps forward continuously (6.6 ± 0.8 cm s^{-1}) after a press on its tail. Both are

[1]Robotics Institute and State Key Laboratory of Mechanical System and Vibration, School of Mechanical Engineering, Shanghai Jiao Tong University, Shanghai 200240, China. [2]Meta Robotics Institute, Shanghai Jiao Tong University, Shanghai 200240, China.
*Corresponding author. Email: guguoying@sjtu.edu.cn (G.G.); mexyzhu@sjtu.edu.cn (X.Z.)

fully soft and electronics-free and achieve intelligent control under a constant-pressure air supply.

RESULTS

Design and working principle of BFMs

A BFM typically consists of two partially bonded flat fabric chambers (chamber 1 and chamber 2), embedded with two easily kinked flexible tubes (tube 1 and tube 2), respectively (Fig. 1A, figs. S1 and S2, and Supplementary Text). The two chambers (control pressure: P_1 and P_2) create a bistable actuator, while the two tubes (control pressure: T_1 and T_2) further enable the function of a bistable valve.

Made from flexible yet almost nonstretchable fabric materials, inflated fabric chambers exhibit buckling behavior under bending deformation (*51*, *52*), resulting in a marked reduction in bending stiffness (fig. S3). Therefore, by partially bonding two fabric chambers in an antagonistic arrangement, our BFM exhibits two stable states during inflation (Fig. 1A and movie S1): Either chamber 1 is straight and chamber 2 is buckled (state I), or chamber 2 is straight and chamber 1 is buckled (state II). By controlling P_1 and P_2 to adjust the bending stiffness of the two chambers, the BFM can transition between these stable states. We illustrate the state transition behavior of our BFM with a three-region phase diagram (Fig. 1B), predicted by a simplified model (fig. S4 and Supplementary Text): region ①—monostable (state I), region ②—monostable (state II), and region ③—bistable (state I and II). When the pressure combination is located in region ③ (for instance, P_1 equals P_2), the BFM exhibits bistable characteristics. In this sense, the BFM can stabilize in either state I or state II and can only transition between two stable states under external torque (see the insets in Fig. 1B). When the pressure combination lies within the other two regions (i.e., when the absolute pressure difference between P_1 and P_2 exceeds a critical value ΔP_c), the BFM transitions to the corresponding stable state regardless of its previous state.

As another design consideration, we embed flexible tubes across the buckling regions of both chambers to control airflow (Fig. 1A

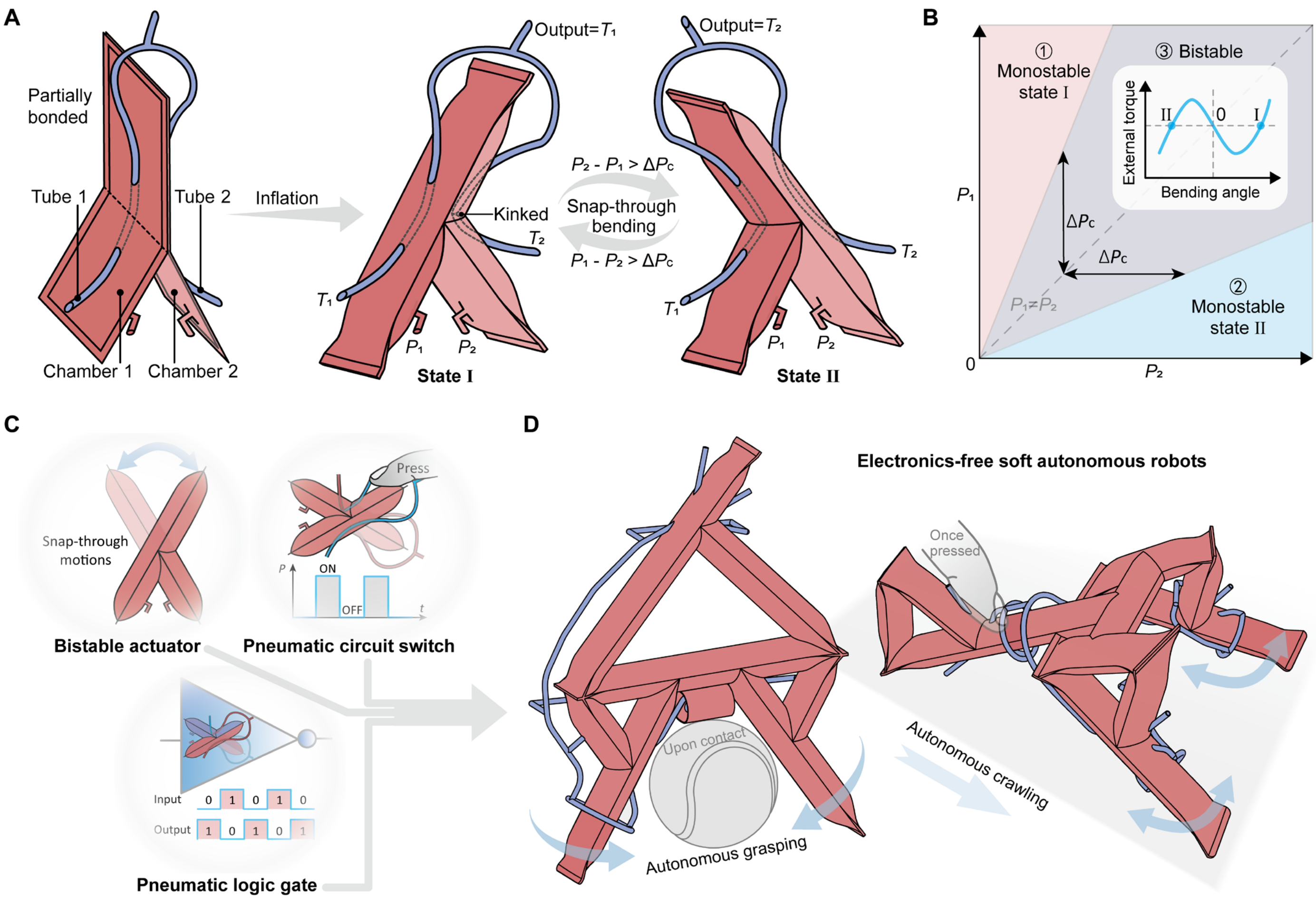

Fig. 1. Design, working principle, multifunctionality, and exemplary applications of bistable fabric mechanisms (BFMs). (**A**) A BFM typically consists of two partially bonded fabric chambers (control pressure: P_1 and P_2) and two embedded tubes (control pressure: T_1 and T_2). By controlling P_1 and P_2, the BFM exhibits two stable states and can transition between these stable states rapidly when the pressure difference exceeds a critical value ΔP_c [as shown in (B)]. In each stable state, one chamber straightens while the other buckles, causing the embedded tubes to be unkinked or kinked to output different pressures, i.e., T_1 or T_2. (**B**) The schematic of the phase diagram of BFMs concerning P_1 and P_2. On the basis of a simplified model (fig. S4 and Supplementary Text), the phase diagram is divided into three regions: region ①—monostable (state I), region ②—monostable (state II), and region ③—bistable (states I and II). (**C**) By configuring the control pressures (i.e., P_1, P_2, T_1, and T_2), BFMs can individually or simultaneously function as bistable actuators, pneumatic circuit switches, and pneumatic logic gates. (**D**) Multifunctional BFMs enable fully soft, electronics-free, and autonomous robots, such as a gripper and a jumping crawler.

and fig. S5). We connect the outlets of the two tubes to form the final output while configuring their inlets with two control pressures (T_1 and T_2) to determine the output pressure. In state I, tube 2 is kinked while tube 1 is unkinked, allowing the pressure T_1 to be transmitted to the output. In state II, tube 1 is kinked while tube 2 is unkinked, permitting the pressure T_2 to be transmitted to the output.

Therefore, our BFMs are essentially soft modules that merge bistable actuators and valves. By configuring the control pressures, i.e., P_1, P_2, T_1, and T_2, our BFMs can function as various pneumatic actuators and control modules, including bistable actuators, PCSs, and pneumatic logic gates (Fig. 1C). These multifunctional BFMs further provide a platform to design electronics-free soft autonomous robots (Fig. 1D).

Characterization of BFMs

We next characterize the bistability, state transition conditions, and actuation performances of BFMs. On the basis of the prior experimental results (fig. S6, A and B), we notice that the embedded tubes have little influence on the mechanical properties of BFMs, which are ignored in the following characterization tests for simplicity.

To demonstrate the bistability, we first characterize the torque-angle relations of our BFMs when $P_1 = P_2 = P$ (see Materials and Methods and movie S1 for characterization details). The results show that the torque-angle curves are almost centrosymmetric and similar to those of typical bistable designs (*45*) (Fig. 2A). Thus, the BFMs have local minimal energy at stable states I and

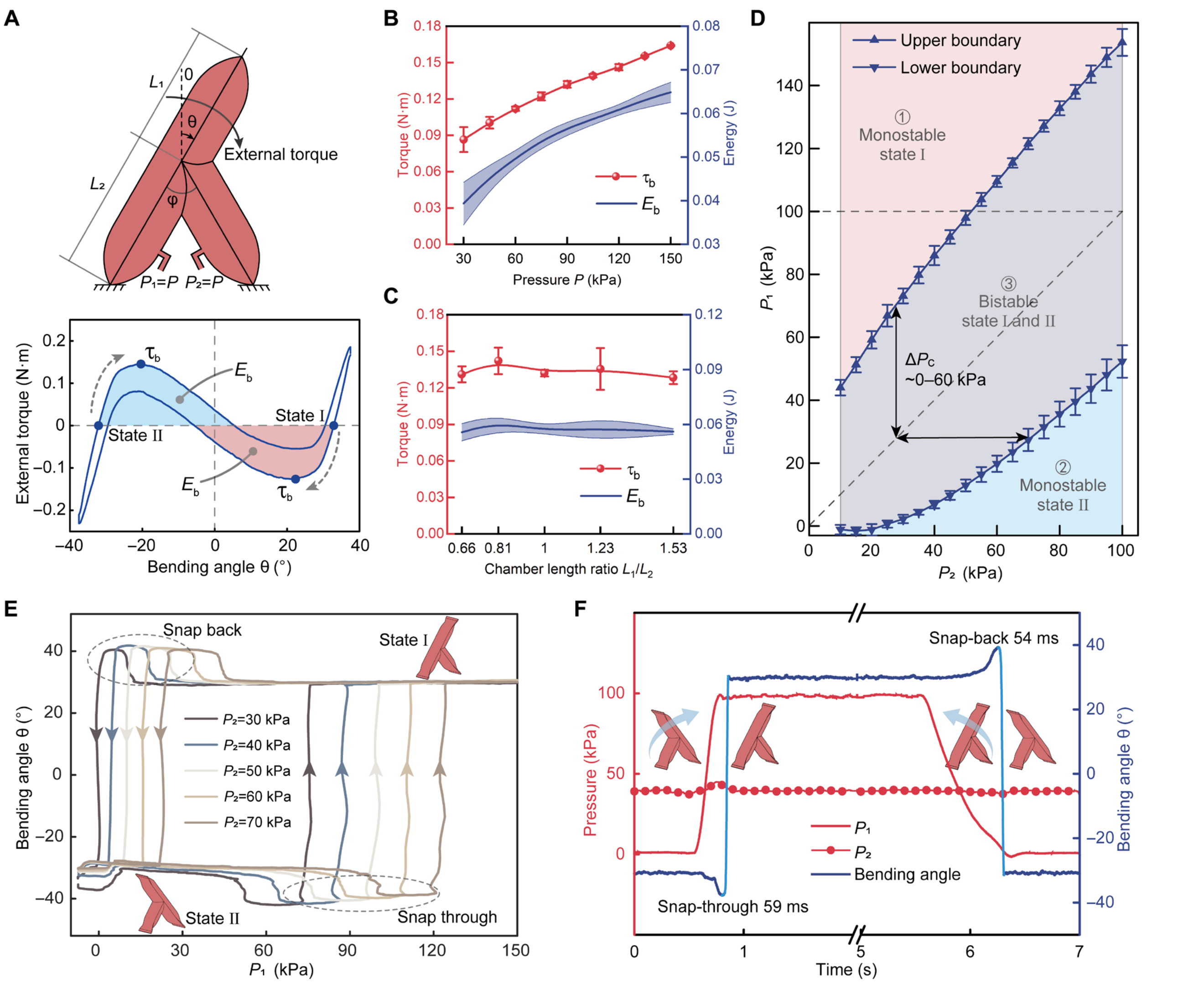

Fig. 2. Characterization of BFMs. (**A**) Exemplary torque-angle relations ($P_1 = P_2 = P = 90$ kPa) demonstrate the bistability of BFMs. BFMs need to overcome the torque barrier τ_b and energy barrier E_b to transition between stable states. (**B**) τ_b and E_b can be tuned by adjusting the actuation pressure P. (**C**) τ_b and E_b rarely vary with the length ratio L_1/L_2 in the measured ranges, showing that this bistability is a local effect. (**D**) Experimentally measured phase diagram of the BFMs. The critical pressure differences ΔP_c ranges between 0 and 60 kPa. When the pressure combination changes across the boundaries, the BFM transitions to corresponding stable states rapidly. (**E**) To simplify the control, P_2 is fixed to a reference pressure and P_1 is controlled to transition between stable states. These snap-through pressures and snap-back pressures are tunable. (**F**) Stimulated by an approximate step pressure, our BFM bends more than 70° within 60 ms, making it an effective bistable actuator for fast bending actuation (more than 1166° s^{-1}). All these presented deviations or error bars are SDs (±SD) in this work.

II. In this sense, our BFMs need to overcome the torque barrier τ_b and energy barrier E_b for transitions between these stable states. By adjusting actuation pressure P, chamber width w, and open angle φ, we can tune τ_b and E_b to make BFMs more stable or sensitive (Fig. 2B; fig. S6, C and D; and Supplementary Text). As shown in Fig. 2C, we can see that τ_b and E_b remain almost constant with the increase of length ratio L_1/L_2, indicating that this bistability is a local effect. To further demonstrate the local effect, we can extend BFMs to other bistable, tristable, and multistable structures by selectively bonding parts of several fabric chambers (fig. S7 and movie S2).

To quantitatively analyze the state transition conditions, we characterize the phase diagram of our BFMs with varying P_1 and P_2 (see fig. S8 and Materials and Methods for characterization details). We can see that the bistable region ③ is bounded by two state transition boundaries, which are roughly symmetric about the line of $P_1 = P_2$ (Fig. 2D). The critical pressure difference ΔP_c to reach the other two monostable regions ① and ② typically ranges between 0 and 60 kPa and enlarges with the increase of P_1 and P_2 due to the growing energy barrier. To simplify the control of state transitions, we fix P_2 to a reference pressure (30 to 70 kPa) while controlling P_1 to vary the pressure combination (Fig. 2E). When P_1 increases to the upper boundary or decreases to the lower boundary in Fig. 2D, our BFMs snap through from state II to state I or snap back from state I to state II (Fig. 2E). These snap-through pressures and snap-back pressures concerning P_1 are tunable by varying the fixed P_2.

Because of the snap-through bending motions during state transitions, our BFMs are inherently capable of functioning as bistable actuators. In the step response tests, the BFMs can bend more than 70° within 60 ms, equivalent to a bending speed of more than 1166° s^{-1} (Fig. 2F). When blocked at the bending angle of 20°, the BFM generates an impact force of approximately 8 N (fig. S9 and Supplementary Text). With the sweep-frequency tests, the BFM can achieve bidirectional bending motions (like a fishtail) up to 1.8 Hz, a limit primarily imposed by the pneumatic hardware (fig. S10, movie S1, and Supplementary Text). In the cyclic tests, the BFM maintains effective actuation capabilities after 10,000 cycles without permanent damage or air leakage (fig. S11 and Supplementary Text). These results demonstrate the excellent actuation performances and robust longevity of our BFMs.

Pneumatic circuit switches

With the above design and characterization results, we can create diverse soft pneumatic control modules by configuring the control pressures of BFMs, i.e., P_1, P_2, T_1, and T_2. As the first example, we develop various PCSs that regulate output pressure in response to external torque or displacement, thus enabling interaction control of pneumatic soft robots.

Figure 3A shows the design and working principle of a three-way two-state PCS, which features three air ports and two operating states, based on a typical BFM. In this PCS, we configure both chambers with a reference pressure to create a passive bistable structure, i.e., $P_1 = P_2 = P_{ref}$ (40 kPa). We connect the inlet of tube 1 to the air supply, i.e., $T_1 = P_{high}$ (90 kPa), and the inlet of tube 2 to the atmosphere, i.e., $T_2 = P_{atm}$ (0 kPa). By applying an external torque, the PCS can switch its output pressure between P_{high} (state I) and P_{atm} (state II). When the external torque is removed, the PCS can maintain the current output pressure (fig. S12A and movie S3).

Varying the number of chambers and tubes can extend the design of PCSs. For example, by applying a similar configuration to a tristable fabric mechanism, we can create a three-way three-state PCS (Fig. 3B). When operating under an air supply with fluctuant pressure, e.g., $P_{high} = 70 \pm 6$ kPa, this PCS can connect to the air supply to output P_{high} (state I), the atmosphere to output P_{atm} (state III), and none of them to hold pressure (state II) (fig. S12B and movie S3). In addition, by embedding two pairs of tubes into one BFM, we can create a four-way two-state PCS with two opposite output pressures (Fig. 3C). This PCS is able to control a pair of antagonistic actuators, such as the fabric-based pneumatic actuators for soft assistive gloves in our previous work (*14*) (fig. S12C and movie S3).

Beyond on/off controls, we can configure the BFM as a proportional PCS for continuous control (Fig. 3D and Supplementary Text). To this end, chamber 2 is connected to the air supply, i.e., $P_2 = P_{high}$ (90 kPa), while other configurations resemble the three-way two-state PCSs. In such a configuration, this PCS exhibits monostability (state II) and transduces bending angles into continuous output pressures by partially connecting to the air supply and partially disconnecting from the atmosphere. Therefore, this proportional PCS integrates the sensing and control capabilities and can enable continuous pressure control of soft actuators, such as the soft finger in our previous work (*12*) (fig. S12D and movie S3).

Pneumatic logic gates

As the second example, we develop various pneumatic logic gates by assigning inputs that toggle between P_{high} and P_{atm} based on the configurations of three-way two-state PCSs. To ensure the state transitions occur when P_{ref} is set to 40 kPa, P_{high} should be greater than the corresponding snap-through pressure, which is approximately 80 kPa (see Fig. 2E). For convenience, we set P_{high} to 100 kPa and use it to represent Boolean 1, while P_{atm} (0 kPa) is used to represent Boolean 0.

Assigning chamber 2 as an input (P_2 = input), the BFM behaves like a NOT gate to invert the input pressures (Fig. 4A, fig. S13A, and movie S4). Using chamber 1 as an input (P_1 = input), the BFM is analogous to a buffer (BUF) gate (Fig. 4B, fig. S13B, and movie S4). This BUF gate does not alter logic but can filter or amplify the input pressures (fig. S13, C and D). Treating chamber 1 and the inlet of tube 1 as input 1 and input 2 (P_1 = input 1; T_1 = input 2), an AND gate is created (Fig. 4C, fig. S13E, and movie S4). Treating the inlet of tube 2 and chamber 1 as input 1 and input 2 (T_2 = input 1; P_1 = input 2), an OR gate is achieved (Fig. 4D, fig. S13F, and movie S4). These gates form a functionally complete set of pneumatic logic gates, providing a platform to achieve the Boolean operations for the autonomous control of pneumatic soft robots (*28*).

Pneumatic oscillators

On the basis of the above NOT gates, we proceed to design pneumatic oscillators that generate periodic pressure oscillations and motion oscillations under constant input. We realize a one-channel oscillator by connecting the output and input of a NOT gate in a

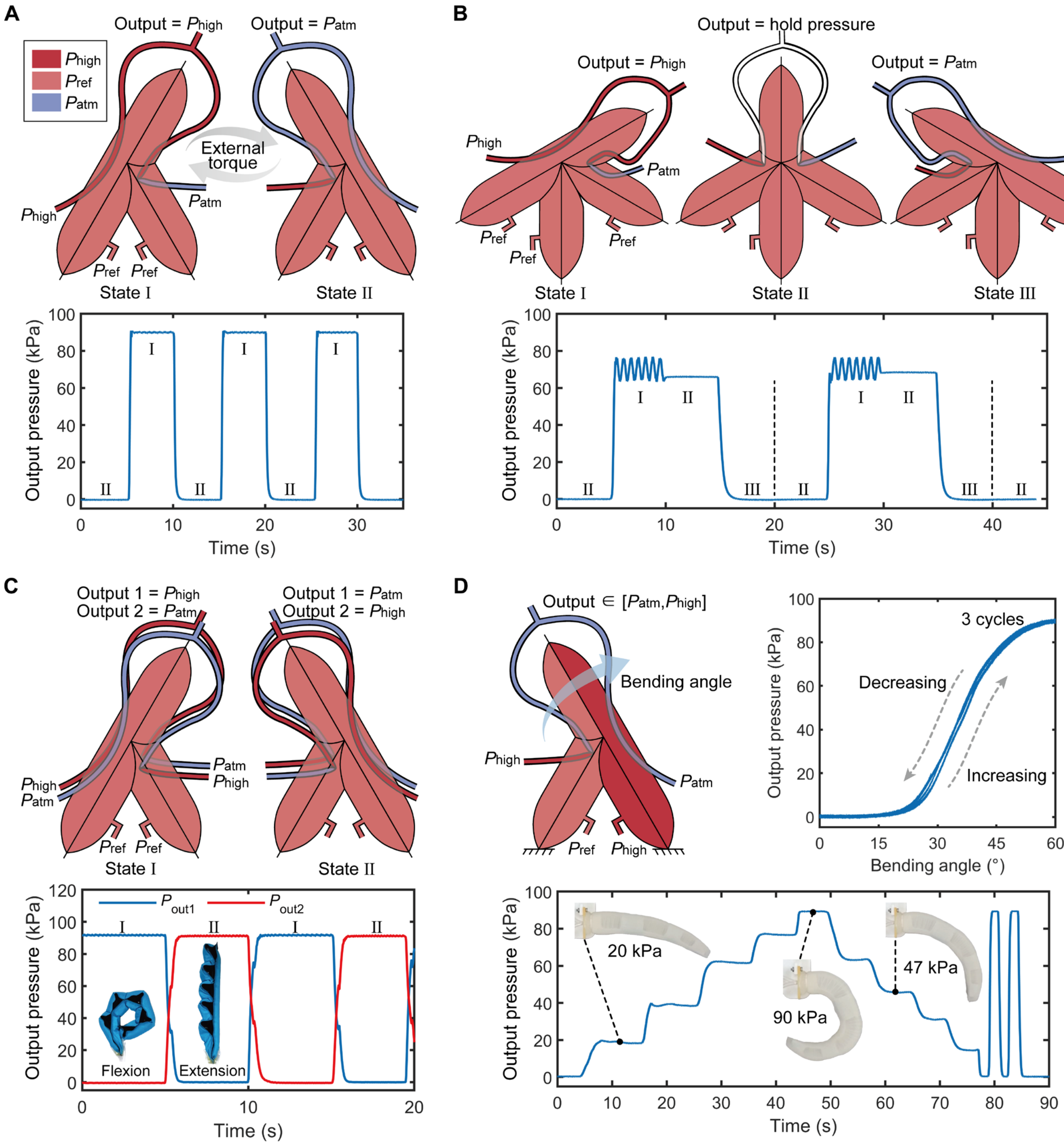

Fig. 3. Pneumatic circuit switches. Create various PCSs by configuring the control pressures of the BFMs using supplied pressure P_{high}, reference pressure P_{ref}, and atmospheric pressure P_{atm}. (**A**) Three-way two-state PCS configuration. External torque can switch the output to connect to either the air supply or the atmosphere. (**B**) Three-way three-state PCS configuration. Besides connecting to the air supply or the atmosphere, the output can hold pressure by disconnecting from both of them. In this experiment, the air supply is programmed to fluctuate with a pressure of $P_{high} = 70 \pm 6$ kPa. (**C**) Four-way two-state PCS configuration. With two pairs of tubes embedded in the chambers, a single PCS can output two opposite pressures. This PCS can control a pair of antagonistic actuators for flexion and extension. (**D**) Proportional PCS configuration. This PCS exhibits monostability and can transduce the bending angles into continuous output pressures to control soft actuators precisely.

feedback way (Fig. 5A, fig. S14A, and movie S5). Powered by a constant-pressure air supply, this oscillator experiences rapid alternating inflation and deflation in its chamber 2 due to structural intelligence (Fig. 5, A and B), outputting oscillating pressures (Fig. 5C) and oscillatory bending motions (Fig. 5D). The oscillating pressures are determined by the snap-through and snap-back pressures, which can be tuned by adjusting the reference pressure (Fig. 2E). When blocked at the bending angle of 20°, this oscillator generates an oscillatory impact force of approximately 7.5 N (fig. S14C). As shown in Fig. 5E, the oscillation frequency increases as the supplied pressure P_{high} increases, which is attributed to the decrease in inflation time as P_{high} increases (fig. S14D and Supplementary Text).

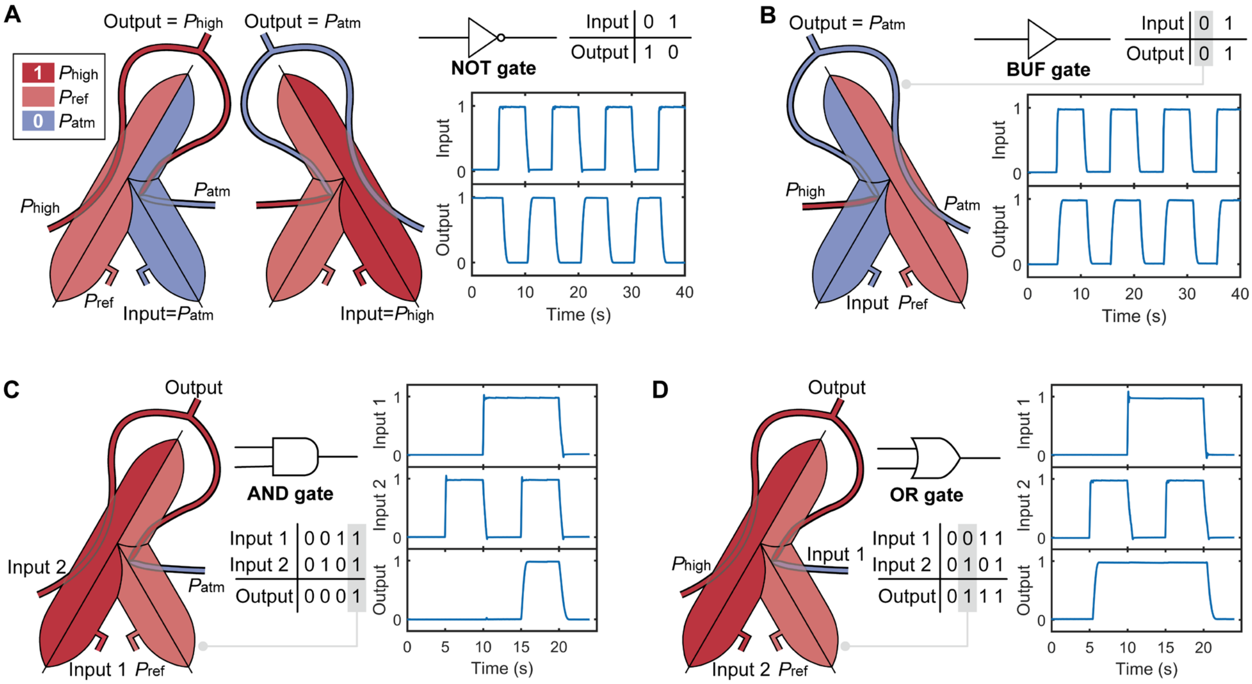

Fig. 4. Pneumatic logic gates. Develop pneumatic logic gates by assigning inputs among the control pressures of the BFMs. The supplied pressure P_{high} is regarded as Boolean 1 while the atmospheric pressure P_{atm} is regarded as Boolean 0. P_{high} and P_{ref} are selected to ensure the state transitions occur. (**A**) Configuration and behaviors of the NOT gate. (**B**) Configuration and behaviors of the buffer (BUF) gate. (**C**) Configuration and behaviors of the AND gate. (**D**) Configuration and behaviors of the OR gate.

In contrast, the oscillation frequency decreases as the open angle φ increases, which can be explained by the increase in the energy barrier as φ increases (fig. S6D). In our experiments, the maximum oscillation frequency observed is 4.6 Hz. Further, we develop a three-channel oscillator by connecting three NOT gates into a loop (Fig. 5F and fig. S14E). This oscillator can output rhythmic motions and three channels of oscillating pressure with approximately 120° phase difference between each channel (Fig. 5G and movie S5). To keep the open angle in practical application, we can lengthen the chambers of BFMs for self-fixation, such as the butterfly-like oscillators (fig. S15 and movie S5). These results demonstrate that our BFMs can multiplex the functions of bistable actuators and pneumatic logic gates to develop integrated, compact, and intelligent actuators.

Electronics-free soft autonomous gripper

In the following, we demonstrate that we can use BFMs as modules to construct electronics-free soft autonomous robots. We first develop a soft gripper (29.7 g) capable of detecting objects and performing dynamic grasping autonomously (Fig. 6A and fig. S16). This gripper employs three BFMs with distinct functions: one acts as a three-way two-state PCS, another serves as a bistable actuator (finger), and the third functions simultaneously as a NOT gate and a bistable actuator (finger). In addition, this gripper contains a custom-designed contact switch, embedding a ring-shaped silicone tube into a cylindrical fabric shell (Fig. 6B). The contact switch normally allows the airflow to pass through but blocks it when contacted. Integrated into the soft gripper, the contact switch requires a normal force of approximately 1.7 N to trigger the grasping behavior (Fig. 6C, movie S6, and Supplementary Text). The three BFMs and the contact switch are heat-pressed onto another horizontal fabric chamber to form the soft gripper (fig. S16). In this application, P_{high} and P_{ref} are set to 120 and 40 kPa, respectively, and the primary airflow passages are depicted using white dashed lines in Fig. 6A.

The operation process of the soft gripper contains four stages (Fig. 6D and movie S6): (i) standby, (ii) contact and grasp, (iii) hold, and (iv) release. In the standby stage, the gripper remains open with the PCS connected to the air supply, allowing high-pressure airflow to vent through the contact switch. In the contact and grasp stage, the contact switch is mechanically pressed to stop venting so that the inner pressure of the gripper (P_{inner}) increases. When P_{inner} reaches the snap-through pressure to trigger the bistable fingers, the gripper grasps the object and blocks the airflow passage between the contact switch and the air supply at the same time (using the NOT gate behaviors). In the hold stage, the gripper steadily grasps the object whether the contact switch is pressed or not. In the final stage, manually switching the PCS to connect to the atmosphere can release the object. After each operation cycle, the PCS is reset for subsequent grasping.

We then showcase that this gripper can steadily grasp objects of various shapes, including balls, cuboids, cylinders, and irregular ones (fig. S17 and movie S6). Notably, the gripper autonomously captures a moving iron ball (0.83 m s^{-1}; 234 g) on impact, owing to the fast actuation of the bistable fingers (Fig. 6E and movie S6). These results show the advancements of our soft autonomous gripper and validate the effectiveness of our BFM-based design method.

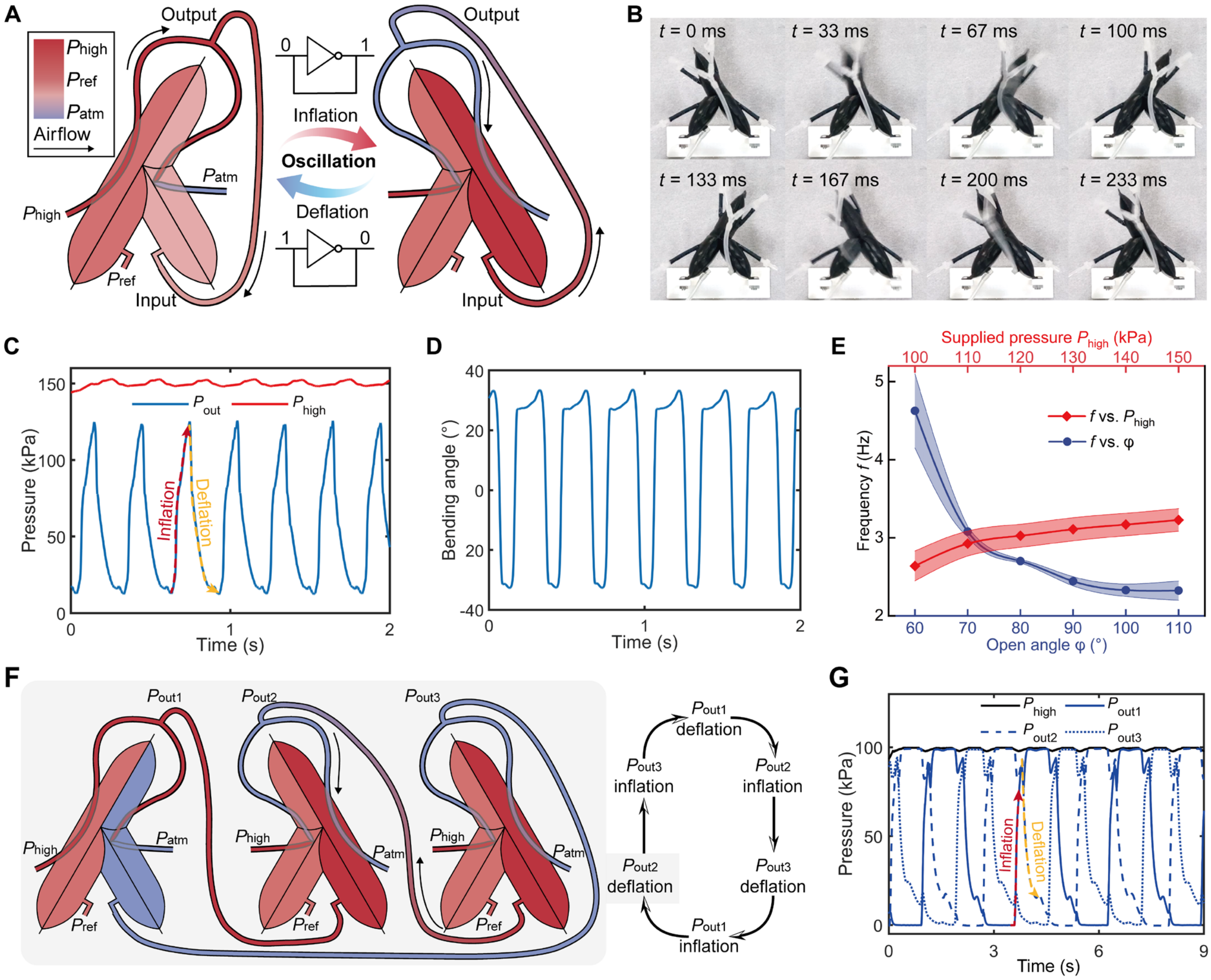

Fig. 5. Pneumatic oscillators. Develop pneumatic oscillators based on the NOT gates. (**A**) A one-channel oscillator is created by connecting the output and input of a NOT gate in a feedback way. (**B**) Photographs of the oscillator during oscillation. (**C**) The oscillating pressure output and (**D**) the oscillatory bending motions when P_{high} = 150 kPa and P_{ref} = 50 kPa (frequency = 3.34 Hz). (**E**) Influences of P_{high} and open angle φ on the oscillation frequency. (**F**) The working principle of the three-channel oscillator. Each cycle contains six steps. The schematic shows the deflation of P_{out2}. (**G**) The oscillating pressure outputs of the three-channel oscillator. These three output pressures lag 120° phase in turn.

Electronics-free soft autonomous crawler

In the second robotic application, we design a soft crawler (33.9 g) that moves forward autonomously after a press on its tail (Fig. 7A and fig. S18). This crawler comprises three BFMs. One BFM positioned at the tail functions as a three-way two-state PCS, with its bonded chambers lengthened to form the robot body. The other two BFMs attached to the body (serving as the robot legs) function as one-channel oscillators. In this application, P_{high} and P_{ref} are set to 70 and 30 kPa, respectively, to ensure that this lightweight robot moves stably, and the primary airflow passages are depicted using white dashed lines in the side view in Fig. 7A.

The oscillators endow the crawler with continuous forward jumping gaits (Fig. 7B and movie S7). At the beginning of each step, the robot legs are at approximately 30° to the ground and their respective chamber 2 is inflating. When inflated to the snap-through pressure, the robot legs generate fast bending motions to flap the ground, resulting in forward jumping gaits. After landing on the ground, the robot legs are almost perpendicular to the ground and their respective chamber 2 is then deflating to generate snap-back bending motions. As the tips of the legs are smoother than the tail, the robot legs slide forward to complete a crawling step Δ*L*. Therefore, the crawler can achieve autonomous crawling powered by one constant-pressure air supply. Moreover, the three-way two-state PCS at the tail can sense external stimuli to control the oscillators to connect to the air supply or the atmosphere, which provides the crawler with interaction capabilities.

The crawler demonstrates intelligent operation with integrated autonomous control and interaction control (Fig. 7C and movie S7). Initially, the PCS connects to the atmosphere, keeping the crawler stationary. With a manual press at the robot tail, the PCS connects to the air supply and the crawler starts to move forward. Subsequently, the crawler autonomously crawls to the destination with an average speed of 6.6 ± 0.8 cm s^{-1} (0.357 ± 0.043 BL s^{-1}) and a power consumption of 2.47 W (Fig. 7D and Supplementary Text). Finally, the crawler can be stopped with a reverse press to reset the PCS. In addition to manual press, we demonstrate that the soft

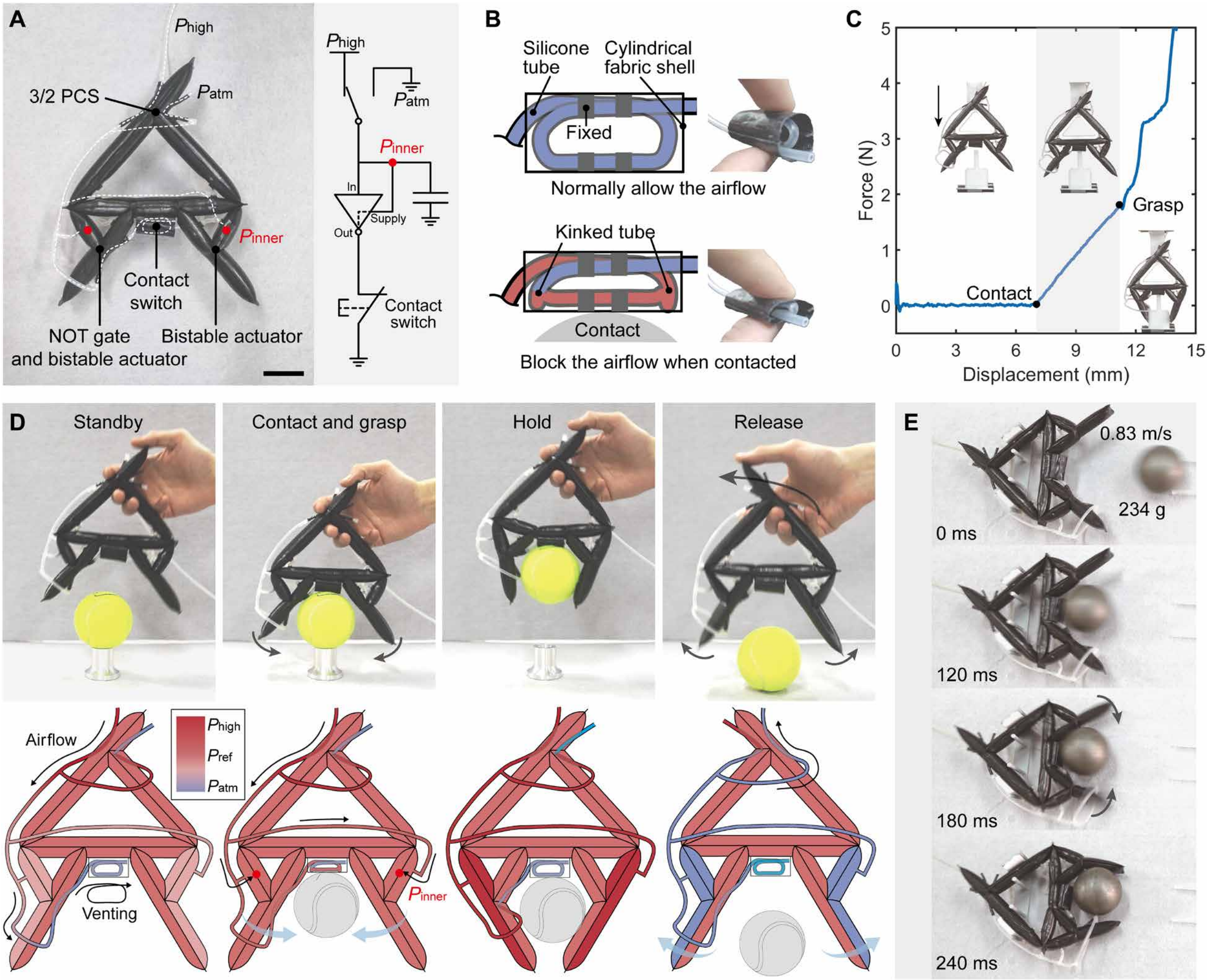

Fig. 6. An electronics-free soft autonomous gripper. (**A**) Components and analogous circuit diagram of the soft gripper. Scale bar, 3 cm. (**B**) Structure and working principle of the contact switch. (**C**) Triggering force test. The grasping behavior is triggered when the contact switch is pressed approximately 4 mm (approximately 1.7 N). (**D**) Photographs and schematics of the soft gripper in the operation process. (**E**) Because of the fast actuation of the bistable actuators, the soft gripper can autonomously capture a moving iron ball. In this application, $P_{high} = 120$ kPa and $P_{ref} = 40$ kPa.

crawler can automatically start when its tail is struck by a falling load (movie S7). This remarkable crawler highlights the versatility of our BFM-based design method and its capabilities in autonomous locomotion.

DISCUSSION

Bistable structures have been successfully used in developing soft actuators with fast actuation or soft valves for electronics-free control. However, achieving them both in a unified and compact design remains elusive. Herein, we present a class of BFMs with embedded pneumatic control components, capable of functioning as various soft actuators and control modules, including bistable actuators, PCSs, and pneumatic logic gates. We also demonstrate that our BFMs can multiplex their actuation and control capabilities to develop intelligent oscillators, which directly produce oscillatory bending motions up to 4.6 Hz. Therefore, the BFMs can be used as modules to construct electronics-free soft autonomous robots, such as the gripper and the crawler developed in this work. Notably, these robots primarily contain fabric and tube materials and achieve intelligent operation powered by one constant air supply.

Different from most pneumatic soft bistable actuators (*46*–*49*), our BFMs are fully soft, simple, and compact, seamlessly integrating pneumatic actuators and bistable structures. Compared with existing soft control modules (table S1), our BFMs demonstrate not only comprehensive pneumatic control capabilities but also direct actuation capabilities. On the basis of our experiments, the BFMs can operate at pressures up to 150 kPa, which meets the requirements for most pneumatic soft robots. In addition, our BFMs are lightweight, low-cost, foldable, scalable, and easily fabricated with heat-sealing/pressing methods. To highlight these advantages, our developed gripper and crawler are fully soft and primarily use BFMs for actuation and control. However, we should mention that the BFMs require an auxiliary reference pressure (P_{ref}), as fabric chambers exhibit almost no bending stiffness when unpressurized. The reference pressure, although increasing complexity, also enhances tunability. Although the

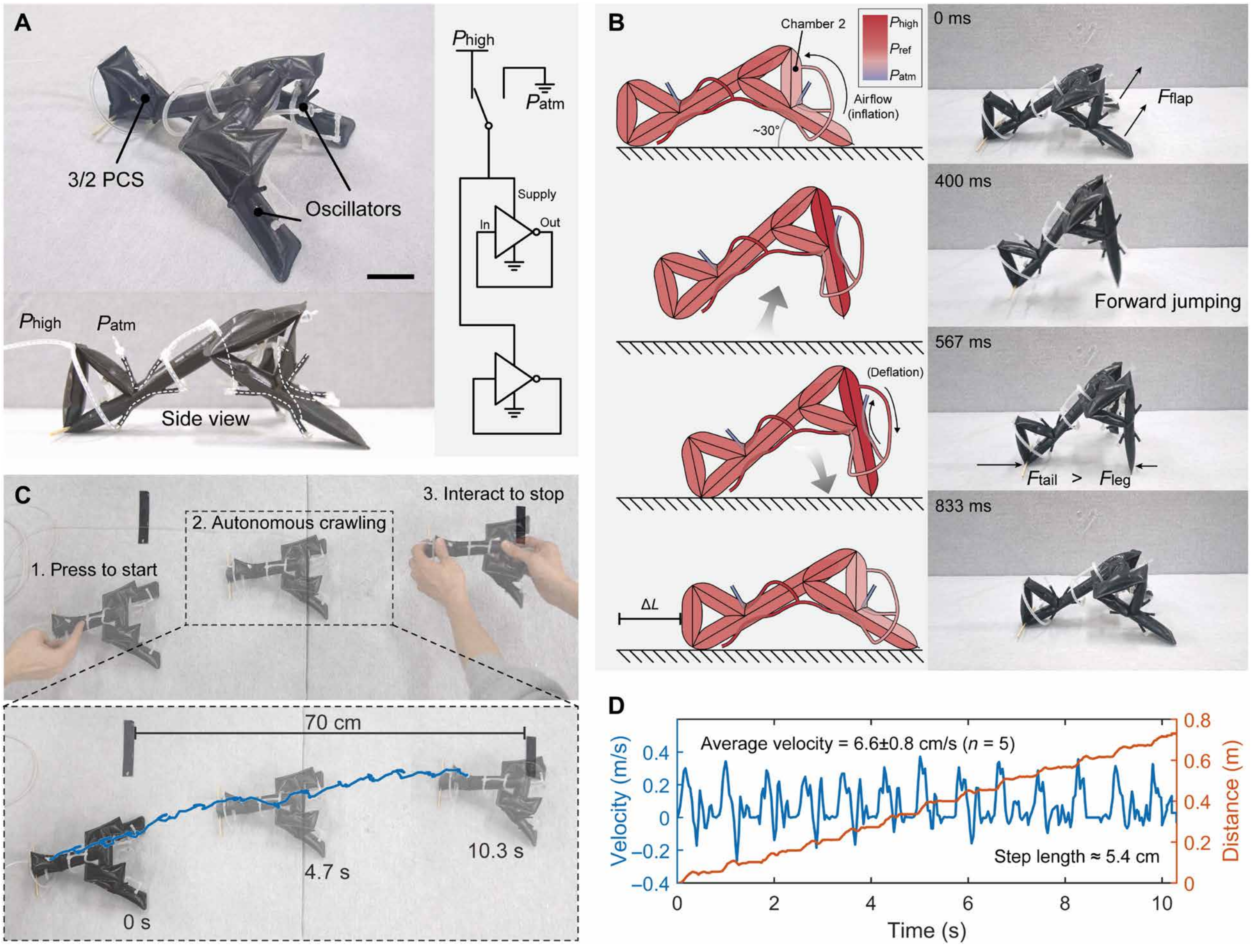

Fig. 7. An electronics-free soft autonomous crawler. (**A**) Components and analogous circuit diagram of the soft crawler. Scale bar, 3 cm. (**B**) Gait schematics and photographs of the soft crawler when performing autonomous crawling (side view). The crawler uses continuous forward jumping gaits to achieve movement. (**C**) The intelligent operation process of the soft crawler (top view). (**D**) The average crawling speed is 6.6 ± 0.8 cm s^{-1} (0.357 ± 0.043 BL s^{-1}). In this application, $P_{high} = 70$ kPa and $P_{ref} = 30$ kPa.

air supply in this work still needs traditional air pumps and pressure regulators, these components could be replaced with soft power devices in the future. Moving forward, many opportunities exist in exploring the applications of BFMs. For example, the proportional PCS can be integrated with human joint (such as finger, wrist, and elbow) to enable real-time control of pneumatic soft robots or assistive wearable devices based on users' motions.

In summary, our BFM-based modules and robots take a step toward entirely soft, self-contained, electronics-free, and autonomous robotic systems. Moreover, we anticipate that our design method of partially bonding chambers and embedding tubes will inspire future research in multistable, reconfigurable, and intelligent structures, actuators, and robots.

MATERIALS AND METHODS

Materials and fabrication of BFMs

Primary materials (fig. S1 and Supplementary Text) comprising BFMs are 150D polyester fabrics with thermoplastic polyurethane (TPU) coated on both sides (0.34 mm; Suzhou Caveman Textile Technology Co. Ltd., China), heat-shrinkable tubes (Φ3; Shenzhen Wanjia Electronic Co Ltd., China), nonstick baking paper (0.05 mm; Foshan Nanhai Weiji Kitchen Utensil Co. Ltd., China), and TPU air connector (Φ3; Shenzhen Jianda Handbag Accessories Co. Ltd., China).

The tools used to fabricate BFMs are a laser cutter (VLS 3.50; Universal Laser Systems, USA), a heat press machine (38 × 38 cm; Yiwu Hexin Digital Technology Co. Ltd., China), and a handheld acrylic bending machine (Type A; Jinan Hongyang CNC Machinery Co. Ltd., China). The main fabrication process contains five steps: (i) laser cut the original materials to obtain patterned fabric sheets and baking paper; (ii) every two fabric sheets are heat sealed to create flat fabric chambers; (iii) two fabric chambers are partially bonded to form a bifurcated structure; (iv) insert tubes through reserved tube path holes; and (v) glue the tube path holes. Please see fig. S2 and Supplementary Text for more details.

Pneumatic sources and pressure control

The pneumatic sources and pressure control in this work are based on an oil-free air compressor (OTS-950x2; Taizhou Outstanding Industry & Trade Co. Ltd., China), a customized pressure regulator (12 channels; Deli Group, China), and a programmable controller (microLabBox 1202; dSPACE, Germany). Controlled by the programmable controller, the pressure regulator can output multichannel desired air supply to BFMs, including constant pressure, sinusoidal pressure, and approximate step pressure. The actual pressures in all experiments are recorded by pressure sensors (MPX Series; Freescale Semiconductor, USA).

Torque-angle relation characterization

As shown in fig. S6A, the experimental setup for characterizing the torque-angle relations consists of a three-axis mobile platform with two adjustable fixtures, a torque sensor (TFF400; Futek, USA) coupled with a jig, and a rotary mobile platform driven by a stepper motor (HS2257; Leadshine Co. Ltd., China). For a given BFM specimen, the characterization process includes installation and testing. Installation: Fix the BFM at an open angle φ using the two fixtures on the three-axis mobile platform; adjust the three-axis mobile platform so that the bifurcation of the BFM is coaxial with the torque sensor; use the jig to secure the bonded regions of the BFM; move the rotary mobile platform to zero position (bending angle $\theta = 0°$) and reset the torque sensor. Testing: Connect the two chambers of the BFM to a constant-pressure air supply; program the stepper motor to drive the rotary mobile platform moving at a speed of $1°\ s^{-1}$; record the torque data at a sample frequency of 50 Hz. The bending angle follows a test path: $0° \rightarrow \varphi/2 + 2.5° \rightarrow -\varphi/2 - 2.5° \rightarrow \varphi/2 + 2.5° \rightarrow 0°$. The data in a reciprocating cycle ($\varphi/2 + 2.5° \rightarrow -\varphi/2 - 2.5° \rightarrow \varphi/2 + 2.5°$) are extracted as the torque-angle relation curve (Fig. 2A and movie S1).

Measurement of the state transition boundaries in the phase diagram

The experimental setup for measuring the state transition boundaries in the phase diagram is shown in fig. S8A. The pressures in the two chambers are controlled independently. A laser sensor (HG-C1400-P; Panasonic, Japan) is used to estimate and record the bending angle θ

$$\theta = \arctan \frac{x}{L_0} \tag{1}$$

where L_0 is the constant initial offset length (22 mm) and x is the measured displacement.

We measure the state transition boundaries by varying P_1 at each fixed P_2. The value of P_2 ranges from 10 to 100 kPa with an interval of 5 kPa. For each fixed P_2, P_1 increases from −10 to 160 kPa at a speed of 5 kPa s^{-1} and then decreases back to −10 kPa (fig. S8B). With P_1 varying, the BFM transitions from state II to state I and then transitions back to state II. The points where state transitions occur are the critical pressure combinations in the state transition boundaries in the phase diagram. The BFMs with default geometric parameters (w = 26 mm; φ = 70°; $L_1/L_2 = 1$) are involved in this measurement and three specimens are tested and averaged to reduce random errors.

Supplementary Materials

The PDF file includes:
Supplementary Text
Figs. S1 to S18
Table S1
Legends for movies S1 to S7

Other Supplementary Material for this manuscript includes the following:
Movies S1 to S7

REFERENCES AND NOTES

1. D. Rus, M. T. Tolley, Design, fabrication and control of soft robots. *Nature* **521**, 467–475 (2015).
2. A. D. Marchese, C. D. Onal, D. Rus, Autonomous soft robotic fish capable of escape maneuvers using fluidic elastomer actuators. *Soft Robot.* **1**, 75–87 (2014).
3. Y. Zhang, D. Yang, P. Yan, P. Zhou, J. Zou, G. Gu, Inchworm inspired multimodal soft robots with crawling, climbing, and transitioning locomotion. *IEEE Trans. Robot.* **38**, 1806–1819 (2022).
4. X. Qi, H. Shi, T. Pinto, X. Tan, A novel pneumatic soft snake robot using traveling-wave locomotion in constrained environments. *IEEE Robot. Autom. Lett.* **5**, 1610–1617 (2020).
5. Z. Xie, A. G. Domel, N. An, C. Green, Z. Gong, T. Wang, E. M. Knubben, J. C. Weaver, K. Bertoldi, L. Wen, Octopus arm-inspired tapered soft actuators with suckers for improved grasping. *Soft Robot.* **7**, 639–648 (2020).
6. M. Wehner, R. L. Truby, D. J. Fitzgerald, B. Mosadegh, G. M. Whitesides, J. A. Lewis, R. J. Wood, An integrated design and fabrication strategy for entirely soft, autonomous robots. *Nature* **536**, 451–455 (2016).
7. Y. Hao, S. Biswas, E. W. Hawkes, T. Wang, M. Zhu, L. Wen, Y. Visell, A multimodal, enveloping soft gripper: Shape conformation, bioinspired adhesion, and expansion-driven suction. *IEEE Trans. Robot.* **37**, 350–362 (2021).
8. W. Kim, J. Eom, K.-J. Cho, A dual-origami design that enables the quasisequential deployment and bending motion of soft robots and grippers. *Adv. Intell. Syst.* **4**, 2100176 (2021).
9. Y. Lin, C. Zhang, W. Tang, Z. Jiao, J. Wang, W. Wang, Y. Zhong, P. Zhu, Y. Hu, H. Yang, J. Zou, A bioinspired stress-response strategy for high-speed soft grippers. *Adv. Sci.* **8**, e2102539 (2021).
10. T. J. Jones, E. Jambon-Puillet, J. Marthelot, P. T. Brun, Bubble casting soft robotics. *Nature* **599**, 229–233 (2021).
11. T. Proietti, C. O'Neill, L. Gerez, T. Cole, S. Mendelowitz, K. Nuckols, C. Hohimer, D. Lin, S. Paganoni, C. Walsh, Restoring arm function with a soft robotic wearable for individuals with amyotrophic lateral sclerosis. *Sci. Transl. Med.* **15**, eadd1504 (2023).
12. G. Gu, N. Zhang, H. Xu, S. Lin, Y. Yu, G. Chai, L. Ge, H. Yang, Q. Shao, X. Sheng, X. Zhu, X. Zhao, A soft neuroprosthetic hand providing simultaneous myoelectric control and tactile feedback. *Nat. Biomed. Eng.* **7**, 589–598 (2023).
13. F. Connolly, D. A. Wagner, C. J. Walsh, K. Bertoldi, Sew-free anisotropic textile composites for rapid design and manufacturing of soft wearable robots. *Extreme Mech. Lett.* **27**, 52–58 (2019).
14. M. Feng, D. Yang, G. Gu, High-force fabric-based pneumatic actuators with asymmetric chambers and interference-reinforced structure for soft wearable assistive gloves. *IEEE Robot. Autom. Lett.* **6**, 3105–3111 (2021).
15. D. Yang, M. Feng, G. Gu, High-stroke, high-output-force, fabric-lattice artificial muscles for soft robots. *Adv. Mater.* **36**, e2306928 (2023).
16. M. Feng, D. Yang, C. Majidi, G. Gu, High-speed and low-energy actuation for pneumatic soft robots with internal exhaust air recirculation. *Adv. Intell. Syst.* **5**, 2200257 (2023).
17. M. S. Xavier, C. D. Tawk, A. Zolfagharian, J. Pinskier, D. Howard, T. Young, J. Lai, S. M. Harrison, Y. K. Yong, M. Bodaghi, A. J. Fleming, Soft pneumatic actuators: A review of design, fabrication, modeling, sensing, control and applications. *IEEE Access* **10**, 59442–59485 (2022).
18. F. Connolly, C. J. Walsh, K. Bertoldi, Automatic design of fiber-reinforced soft actuators for trajectory matching. *Proc. Natl. Acad. Sci. U.S.A.* **114**, 51–56 (2016).
19. C. Jiang, D. Wang, B. Zhao, Z. Liao, G. Gu, Modeling and inverse design of bio-inspired multi-segment pneu-net soft manipulators for 3D trajectory motion. *Appl. Phys. Rev.* **8**, 041416 (2021).
20. J. Kwon, S. J. Yoon, Y.-L. Park, Flat inflatable artificial muscles with large stroke and adjustable force–length relations. *IEEE Trans. Robot.* **36**, 743–756 (2020).
21. N. Oh, J.-G. Lee, H. Rodrigue, Torsional pneumatic actuator based on pre-twisted pneumatic tubes for soft robotic manipulators. *IEEE/ASME Trans. Mechatron.* **28**, 3191–3201 (2023).
22. A. Pal, D. Goswami, R. V. Martinez, Elastic energy storage enables rapid and programmable actuation in soft machines. *Adv. Func. Mater.* **30**, 1906603 (2019).
23. M. Feng, D. Yang, L. Ren, G. Wei, G. Gu, X-crossing pneumatic artificial muscles. *Sci. Adv.* **9**, adi7133 (2023).
24. J. A. Tracz, L. Wille, D. Pathiraja, S. V. Kendre, R. Pfisterer, E. Turett, C. K. Abrahamsson, S. E. Root, W.-K. Lee, D. J. Preston, H. J. Jiang, G. M. Whitesides, M. P. Nemitz, Tube-balloon logic for the exploration of fluidic control elements. *IEEE Robot. Autom. Lett.* **7**, 5483–5488 (2022).
25. A. Rajappan, B. Jumet, R. A. Shveda, C. J. Decker, Z. Liu, T. F. Yap, V. Sanchez, D. J. Preston, Logic-enabled textiles. *Proc. Natl. Acad. Sci. U.S.A.* **119**, e2202118119 (2022).
26. Y. Zhai, A. De Boer, J. Yan, B. Shih, M. Faber, J. Speros, R. Gupta, M. T. Tolley, Desktop fabrication of monolithic soft robotic devices with embedded fluidic control circuits. *Sci. Robot.* **8**, eadg3792 (2023).
27. P. Rothemund, A. Ainla, L. Belding, D. J. Preston, S. Kurihara, Z. Suo, G. M. Whitesides, A soft, bistable valve for autonomous control of soft actuators. *Sci. Robot.* **3**, eaar7986 (2018).

28. C. J. Decker, H. J. Jiang, M. P. Nemitz, S. E. Root, A. Rajappan, J. T. Alvarez, J. Tracz, L. Wille, D. J. Preston, G. M. Whitesides, Programmable soft valves for digital and analog control. *Proc. Natl. Acad. Sci. U.S.A.* **119**, e2205922119 (2022).
29. L. C. van Laake, J. de Vries, S. Malek Kani, J. T. B. Overvelde, A fluidic relaxation oscillator for reprogrammable sequential actuation in soft robots. *Matter* **5**, 2898–2917 (2022).
30. L. Jin, Y. Yang, B. O. T. Maldonado, S. D. Lee, N. Figueroa, R. J. Full, S. Yang, Ultrafast, programmable, and electronics-free soft robots enabled by snapping metacaps. *Adv. Intell. Syst.* **5**, 2300039 (2023).
31. N. Vasios, A. J. Gross, S. Soifer, J. T. B. Overvelde, K. Bertoldi, Harnessing viscous flow to simplify the actuation of fluidic soft robots. *Soft. Robot.* **7**, 1–9 (2020).
32. L. Jin, A. E. Forte, K. Bertoldi, Mechanical valves for on-board flow control of inflatable robots. *Adv. Sci.* **8**, e2101941 (2021).
33. D. J. Preston, P. Rothemund, H. J. Jiang, M. P. Nemitz, J. Rawson, Z. Suo, G. M. Whitesides, Digital logic for soft devices. *Proc. Natl. Acad. Sci. U.S.A.* **116**, 7750–7759 (2019).
34. D. J. Preston, H. J. Jiang, V. Sanchez, P. Rothemund, J. Rawson, M. P. Nemitz, W.-K. Lee, Z. Suo, C. J. Walsh, G. M. Whitesides, A soft ring oscillator. *Sci. Robot.* **4**, eaaw5496 (2019).
35. S. Conrad, J. Teichmann, P. Auth, N. Knorr, K. Ulrich, D. Bellin, T. Speck, F. J. Tauber, 3D-printed digital pneumatic logic for the control of soft robotic actuators. *Sci. Robot.* **9**, eadh4060 (2024).
36. J. D. Hubbard, R. Acevedo, K. M. Edwards, A. T. Alsharhan, Z. Wen, J. Landry, K. Wang, S. Schaffer, R. D. Sochol, Fully 3D-printed soft robots with integrated fluidic circuitry. *Sci. Adv.* **7**, eabe5257 (2021).
37. A. A. Stanley, E. S. Roby, S. J. Keller, High-speed fluidic processing circuits for dynamic control of haptic and robotic systems. *Sci. Adv.* **10**, eadl3014 (2024).
38. W.-K. Lee, D. J. Preston, M. P. Nemitz, A. Nagarkar, A. K. MacKeith, B. Gorissen, N. Vasios, V. Sanchez, K. Bertoldi, L. Mahadevan, G. M. Whitesides, A buckling-sheet ring oscillator for electronics-free, multimodal locomotion. *Sci. Robot.* **7**, eabg5812 (2022).
39. J. K. Choe, J. Kim, H. Song, J. Bae, J. Kim, A soft, self-sensing tensile valve for perceptive soft robots. *Nat. Commun.* **14**, 3942 (2023).
40. S. Song, S. Joshi, J. Paik, CMOS-inspired complementary fluidic circuits for soft robots. *Adv. Sci.* **8**, e2100924 (2021).
41. D. Drotman, S. Jadhav, D. Sharp, C. Chan, M. T. Tolley, Electronics-free pneumatic circuits for controlling soft-legged robots. *Sci. Robot.* **6**, eaay2627 (2021).
42. Q. He, R. Yin, Y. Hua, W. Jiao, C. Mo, H. Shu, J. R. Raney, A modular strategy for distributed, embodied control of electronics-free soft robots. *Sci. Adv.* **9**, eade9247 (2023).
43. Z. Jiao, Z. Hu, Y. Shi, K. Xu, F. Lin, P. Zhu, W. Tang, Y. Zhong, H. Yang, J. Zou, Reprogrammable, intelligent soft origami LEGO coupling actuation, computation, and sensing. *Innovation* **5**, 100549 (2024).
44. B. Gorissen, E. Milana, A. Baeyens, E. Broeders, J. Christiaens, K. Collin, D. Reynaerts, M. De Volder, Hardware sequencing of inflatable nonlinear actuators for autonomous soft robots. *Adv. Mater.* **31**, e1804598 (2019).
45. Y. Chi, Y. Li, Y. Zhao, Y. Hong, Y. Tang, J. Yin, Bistable and multistable actuators for soft robots: Structures, materials, and functionalities. *Adv. Mater.* **34**, e2110384 (2022).
46. Y. Chi, Y. Hong, Y. Zhao, Y. Li, J. Yin, Snapping for high-speed and high-efficient butterfly stroke-like soft swimmer. *Sci. Adv.* **8**, eadd3788 (2022).
47. Y. Tang, Y. Chi, J. Sun, T.-H. Huang, O. H. Maghsoudi, A. Spence, J. Zhao, H. Su, J. Yin, Leveraging elastic instabilities for amplified performance: Spine-inspired high-speed and high-force soft robots. *Sci. Adv.* **6**, eaaz6912 (2020).
48. Z. Zhang, X. Ni, H. Wu, M. Sun, G. Bao, H. Wu, S. Jiang, Pneumatically actuated soft gripper with bistable structures. *Soft Robot.* **9**, 57–71 (2022).
49. Q. Guo, Y. Sun, T. Zhang, S. Xie, X. Chen, Z. Zhang, H. Jiang, L. Yang, Bistable insect-scale jumpers with tunable energy barriers for multimodal locomotion. *Adv. Sci.* **11**, e2404404 (2024).
50. S. Wang, L. He, P. Maiolino, Design and characterization of a 3D-printed pneumatically-driven bistable valve with tunable characteristics. *IEEE Robot. Autom. Lett.* **7**, 112–119 (2022).
51. J. Wei, H. Ding, Y. Chai, A. Eriksson, H. Tan, Quasi-static folding and deployment of rigidizable inflatable beams. *Int. J. Solids Strut.* **232**, 111063 (2021).
52. E. M. Haseganu, D. J. Steigmann, Theoretical flexural response of a pressurized cylindrical membrane. *Int. J. Solids Strut.* **31**, 27–50 (1994).

Acknowledgments: We thank L. Wang and J. Li for their discussion in the writing. **Funding:** This work was partially supported by the National Natural Science Foundation of China (grant nos. 52025057, T2293725, and 91948302) and the State Key Laboratory of Mechanical System and Vibration (grant no. MSVZD202401). **Author contributions:** D.Y. conceived the idea and contributed to experiments, data curation, investigation, visualization, and writing. M.F. assisted in experiments, investigation, and writing. J.S. and Y.W. assisted in experiments and writing. J.Z. assisted in writing. G.G. and X.Z. supervised the project and contributed to the design of experiments and writing. All the authors provided feedback and agreed with the final version of the manuscript. **Competing interests:** The authors declare that they have no competing interests. **Data and materials availability:** All data needed to evaluate the conclusions in the paper are present in the paper and/or the Supplementary Materials.

Submitted 3 September 2024
Accepted 31 December 2024
Published 31 January 2025
10.1126/sciadv.ads8734